FULL PAPER

Open Access

Long-term slow slip events with and without tremor activation in the Bungo Channel and Hyuganada, southwest Japan

Hitoshi Hirose[1*] , Takeshi Matsushima[2], Takao Tabei[3] and Takuya Nishimura[4]

Abstract

Slow slip events (SSEs) lasting for approximately 1 year occur every 6–8 years around the Bungo Channel in the southwest Japan subduction zone. The slip time evolution of the latest Bungo Channel SSE that occurred in 2018–2019 has been studied; however, the detailed spatial and temporal relationship between the slip process and other nearby phenomena, such as tectonic tremors and SSEs, is not well understood. Moreover, the migration of such long-term SSEs from Hyuganada to Shikoku through the Bungo Channel has been suggested, but a slip process connecting the SSEs has not been observed. In this study, we utilized 21 continuous global navigation satellite system (GNSS) stations around the Bungo Channel and Hyuganada that have been installed by us since 2014 in addition to GNSS Earth Observation System (GEONET) stations to improve the spatial resolution of such interplate slip. Based on these data, we estimate the spatial and temporal slip evolutions of the major SSE in 2018–2019, which was accompanied by tremor activity in the deep episodic tremor and slip (ETS) zone, and a smaller SSE in 2015–2016 without tremor activity. We show that the slip area of the major SSE overlaps the ETS zone, whereas that of the smaller SSE does not. This strongly suggests that synchronized tremor activity with an SSE requires a slip close to or overlapping the ETS zone. We also show two distinct slip propagation paths from the Oita area during the 2018–2019 sequence: one is a southward propagation to the Miyazaki area, leading to an SSE around the Miyazaki Plain, and the other is an eastward propagation to an area close to Cape Ashizuri, where "invading slip" is proposed to propagate from the ETS zone to a shallower megathrust source area. These slip propagations may be two of fundamental slip modes that connect slow-slip patch-like areas around the Bungo Channel and Hyuganada.

Keywords GNSS, Aseismic slip, Slow earthquakes, Nankai subduction zone, Plate interface
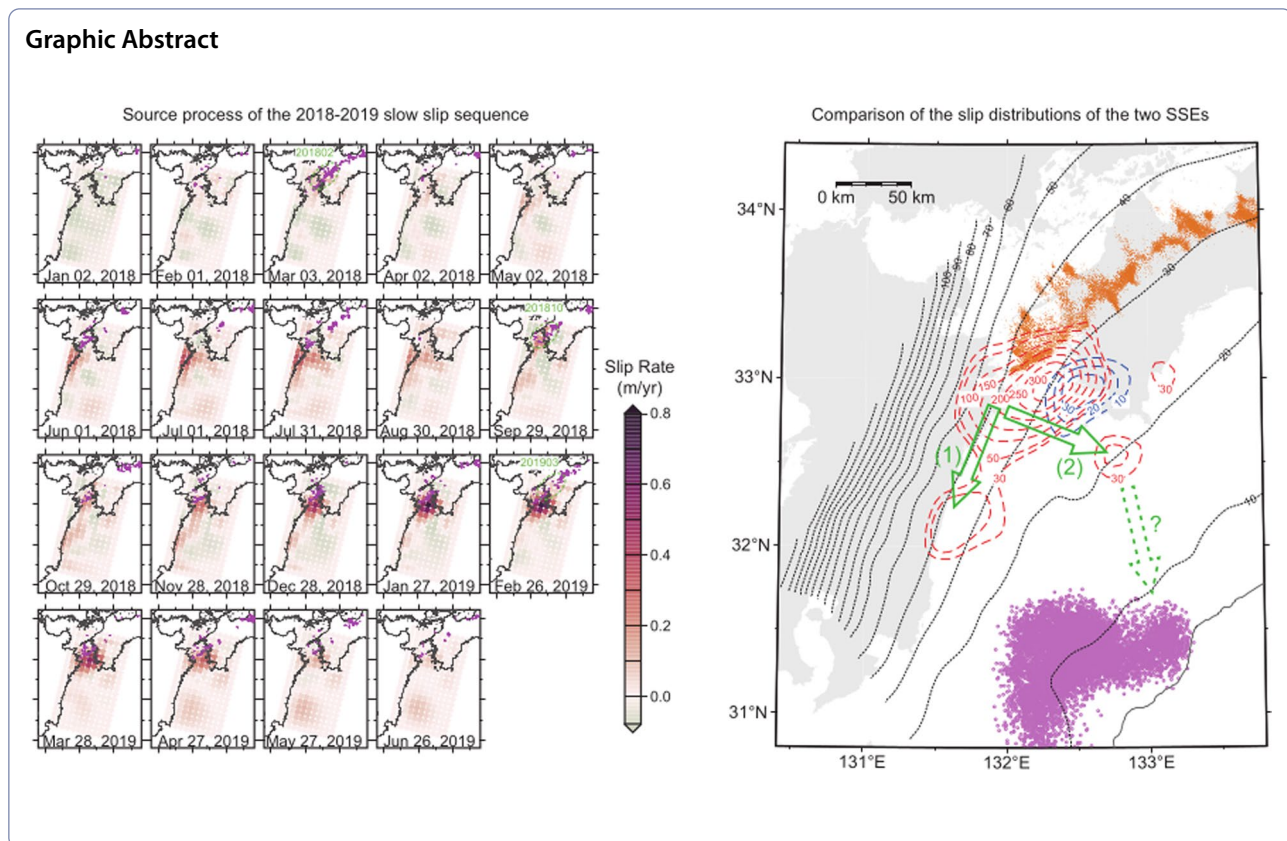
*Correspondence:
Hitoshi Hirose
hitoshi.hirose@ruby.kobe-u.ac.jp
Full list of author information is available at the end of the article

Graphic Abstract

Introduction

In the southwest Japan subduction zone, a wide variety of fast and slow earthquake activities occur in association with the subduction of the Philippine Sea plate along the Nankai Trough (Fig. 1). The adjacent Shikoku area and Kyushu-Hyuganada area show contrasting behaviors of these activities. Around the Shikoku area, megathrust earthquakes larger than magnitude (M) 8 have repeatedly occurred, with recurrence interval of approximately 100–200 years in the shallower part of the subducting plate interface [e.g. Ando (1975); Sagiya and Thatcher (1999)]. At the deeper part (about 30–40 km in depth), tectonic tremor (Obara 2002) and slow slip events (SSEs) occur simultaneously (Obara et al. 2004), termed episodic tremor and slip [ETS; Rogers and Dragert (2003)]. The typical duration of ETS episodes in the western Shikoku area is one week; hence, an SSE that comprises an ETS episode is called a short-term SSE. SSEs that last for several months are located at intermediate depths (approximately 20–30 km) [e.g. Kobayashi (2010, 2012); Takagi et al. (2016, 2019)]. In contrast, off the southeast coast of Kyushu, Hyuganada, earthquakes with M > 8 have not been observed. One of the largest earthquakes in Hyuganada is the M 7.5 1968 Hyuganada earthquake (Yagi et al. 1998). Deep tremor activity in Kyushu is not

as active as that in Shikoku (Ide 2012), but active tremor episodes have been detected in the shallowest part near the Nankai Trough (Yamashita et al. 2015, 2021). These tremors are thought to be a higher-frequency manifestation of very low-frequency earthquakes (VLFEs) in Hyuganada (Obara and Ito 2005; Asano et al. 2008, 2015; Tonegawa et al. 2020). SSEs are also frequently observed along the southeast coast of Kyushu at depths of approximately 30–40 km (Yarai and Ozawa 2013; Nishimura 2014; Ozawa 2017; Takagi et al. 2019; Okada et al. 2022). These include SSEs with longer and shorter duration but they appear to occur at similar locations. Among them, a characteristic activity is the long-term SSEs around the Miyazaki area, which frequently occur once every two or three years (Yarai and Ozawa 2013; Ozawa 2017; Takagi et al. 2019). In addition, repeating earthquakes are observed just updip of the SSE zone at depths of 15–30 km (Yamashita et al. 2012; Uchida et al. 2020).

The Bungo Channel is geographically located between Shikoku and Kyushu and corresponds to a tectonically and seismologically transitional area between Shikoku and Kyushu, where the dip angle of the subducting Philippine Sea plate gradually changes from shallow to steep and the interplate coupling changes from strong to weak [e.g. Yokota et al. (2016); Nishimura et al. (2018); Kimura
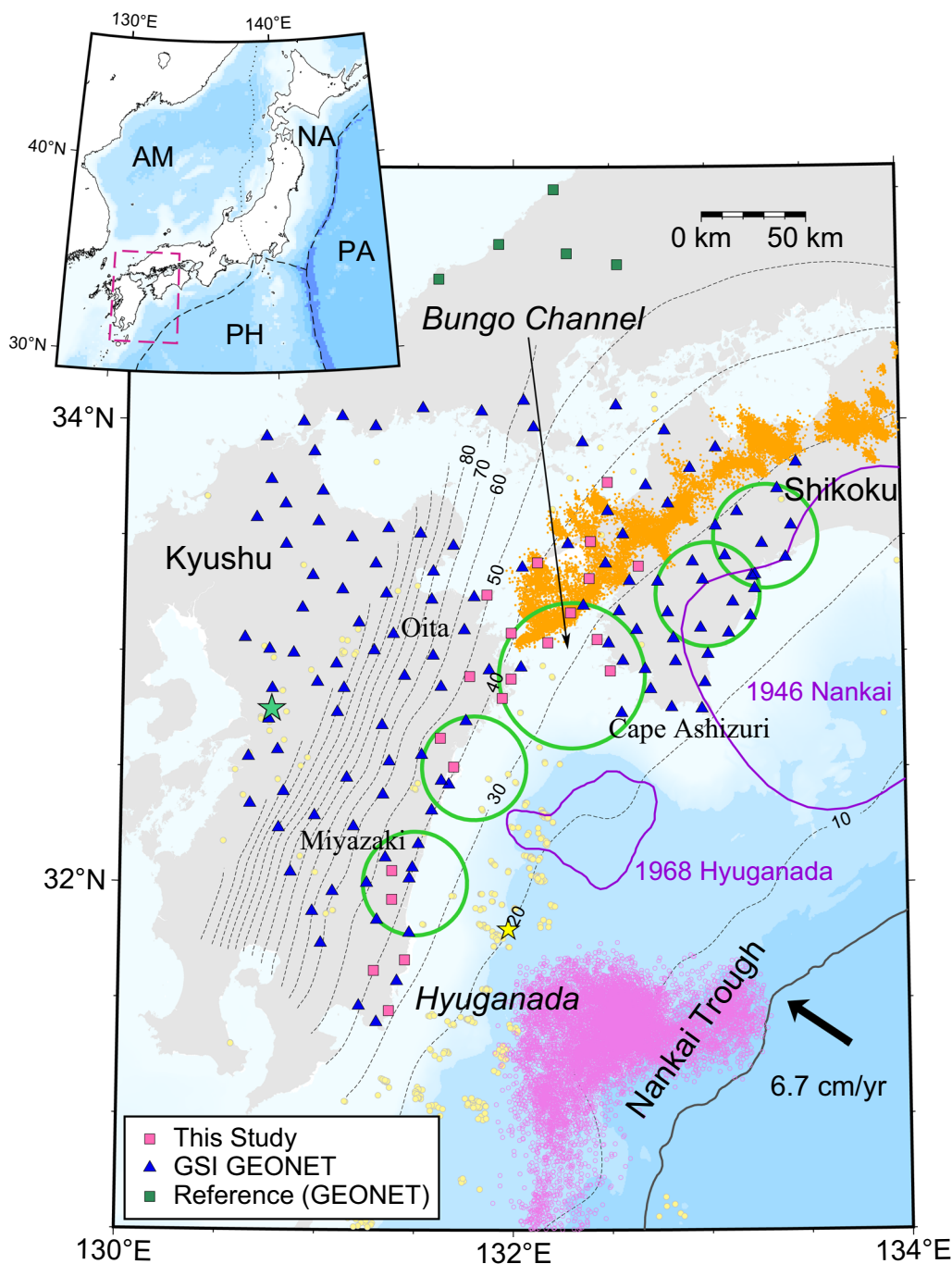
Fig. 1 Index map showing the tectonic settings, seismicity, and station locations in the study area. Pink squares, blue triangles, and green squares represent the GNSS stations installed in this study, GEONET stations used, and reference stations (GEONET) defined, respectively. The solid curve shows the Nankai Trough and broken lines show the plate interface depth contours (digits are depths represented in km). Purple curves represent the rupture areas of the 1946 Nankai earthquake (Sagiya and Thatcher 1999) and the 1968 Hyuganada earthquake (Yagi et al. 1998). Green circles denote source areas of long-term slow slip events (Hirose et al. 1999; Kobayashi 2010, 2012; Yarai and Ozawa 2013; Takagi et al. 2016, 2019). Orange dots show epicenters of deep tremors from the NIED tremor catalog (Maeda and Obara 2009; Obara et al. 2010). Pink circles represent shallow tremors (Yamashita et al. 2015, 2021). Yellow circles show epicenters of repeating earthquakes (Uchida et al. 2020). Green and yellow stars denote the epicenters of the 2016 Kumamoto earthquake and the Hyuganada earthquake in May 2019, respectively. (Inset) Tectonic plate configurations around Japan islands. *NA* North America plate, *PA* Pacific plate, *PH* Philippine Sea plate, and *AM* Amurian plate

Hirose *et al. Earth, Planets and Space* (2023) 75:77

Page 4 of 16

et al. ([2019])]. A characteristic slip phenomenon in the Bungo Channel is long-term SSEs with ~1 year duration, which repeatedly occur with recurrence intervals of 6–8 years in a similar depth range to long-term SSEs in Shikoku and Kyushu [e.g. Hirose et al. ([1999]); Ozawa et al. ([2001], [2020]); Seshimo and Yoshioka ([2022])]. In addition, smaller long-term SSEs occur between the major long-term SSEs [e.g. Ozawa ([2017])]. ETS episodes are also active in the deeper part of the Bungo Channel area, similar to those in Shikoku. However, there is little evidence of the occurrence of a great earthquake updip of the SSE area.

A striking feature of Bungo Channel SSEs is the synchronized activation of deep tremors in the Bungo Channel and shallow VLFEs far south off Cape Ashizuri (Hirose et al. [2010]). As the northernmost part of the SSE fault overlaps the updip part of the ETS zone, the propagation of the slow slip into the ETS zone is suggested to directly trigger the tremor activity. However, the spatial and temporal relationship between a long-term SSE and ETS activity is not well understood because of the lack of a detailed comparison between the spatiotemporal slip evolution of SSEs and tremor activity. Moreover, the relationship between the activity of shallow VLFEs and long-term SSEs is still unknown because of the lack of observation data that are sensitive to offshore slip.

Takagi et al. ([2019]) detected several long-term SSEs in Hyuganada, the Bungo Channel, and Shikoku and demonstrated that the order of occurrence of long-term SSEs in this area was from south to northeast. They interpreted that this behavior was a migration of long-term SSEs. In addition, Uchida et al. ([2020]) showed a couple of northward migration episodes of repeating earthquakes, VLFEs, and SSEs in Hyuganada and the Bungo Channel over a large distance of ~300 km. They suggested that possible slow slip triggering these activities propagated from the southern part of Hyuganada to the ETS zone in the Bungo Channel and Shikoku. However, it is unclear whether such long-distance slip propagation actually exists, whether slip always propagates northward, and whether there are other propagation paths, for example, between the Bungo Channel and the Miyazaki area in Hyuganada and between the Bungo Channel and the area far south off Cape Ashizuri, where VLFE activity occurred during a long-term SSE in the Bungo Channel.

In this study, we estimated the spatial and temporal slip evolutions around the Bungo Channel and Hyuganada

during two time periods: a smaller SSE during 2015–2016, and a sequence of slip episodes during 2018–2019, including a major long-term SSE in the Bungo Channel and a long-term SSE in Miyazaki. Ozawa ([2017]) estimated a time-dependent slow slip from 2013–2016 in the similar area including the smaller SSE based on GEONET [Japan's nationwide GNSS network operated by the Geospatial Information Authority of Japan (GSI)] data, but the relationship between the SSE and a tremor activity in the ETS zone is not discussed. Also, source slip processes of the latest major Bungo Channel SSE during 2018–2019 have been estimated using GEONET data (Ozawa et al. [2020]; Seshimo and Yoshioka [2022]); however, a direct connection to adjacent areas, especially the Hyuganada area is unclear. To improve the spatial resolution of the interplate slip, we have installed continuous GNSS stations around the Bungo Channel and the Miyazaki area since 2014. Based on these data and GEONET data, we obtained the slip distributions of the smaller and major SSEs, and compared their source processes with the tremor activity in the ETS zone. Moreover, we explored slip propagations during the sequence in 2018–2019 to show direct connections not only between slip patch-like areas in the Bungo Channel but also around Hyuganada.

Data
As mentioned above, we installed 21 continuous GNSS stations in Shikoku and Kyushu (pink rectangles in Fig. [1]). These stations are located in regions with sparse existing GEONET stations, particularly in and around the Bungo Channel, where the main slip area of the previous SSEs is located. Most of our stations have commercial power supplies, but some do not. In such a case, a GNSS receiver is powered by solar panels (e.g. station MZNK is located on an uninhabited island in the Bungo Channel, Fig. [2]a).

We used these observed data and the GEONET data provided on the website (https://terras.gsi.go.jp/). Receiver Independent Exchange Format (RINEX) files of these stations were processed to obtain daily coordinates of the stations in IGS14 (International GNSS Service 14) reference frame (http://acc.igs.org/igs-frames.html) by using the GIPSY-OASIS software version 6.4, developed by the Jet Propulsion Laboratory (JPL) (https://gipsy-oasis.jpl.nasa.gov/). We converted the time of the coordinate time series data from Global Positioning System (GPS) time to Japan Standard Time

(See figure on next page.)
Fig. 2 Observed and synthetic displacement time series data for selected stations. **a** Station locations. Open squares and open triangles show GNSS stations used for the SSE in 2015–2016 and for the 2018–2019 sequence, respectively. **b**–**d** Observed (dots) and synthetic (gray lines) data for the SSE in 2015–2016. **e**–**g** Observed (dots) and synthetic (gray lines) data for the 2018–2019 sequence. **b**, **e** East components, **c**, **f** north components, and **d**, **g** vertical components. Vertical dotted lines in (**b**–**d**) represent the origin time of the 2016 Kumamoto earthquake. Note that the vertical scale for the vertical components (**d**, **g**) is different from that for the horizontal components
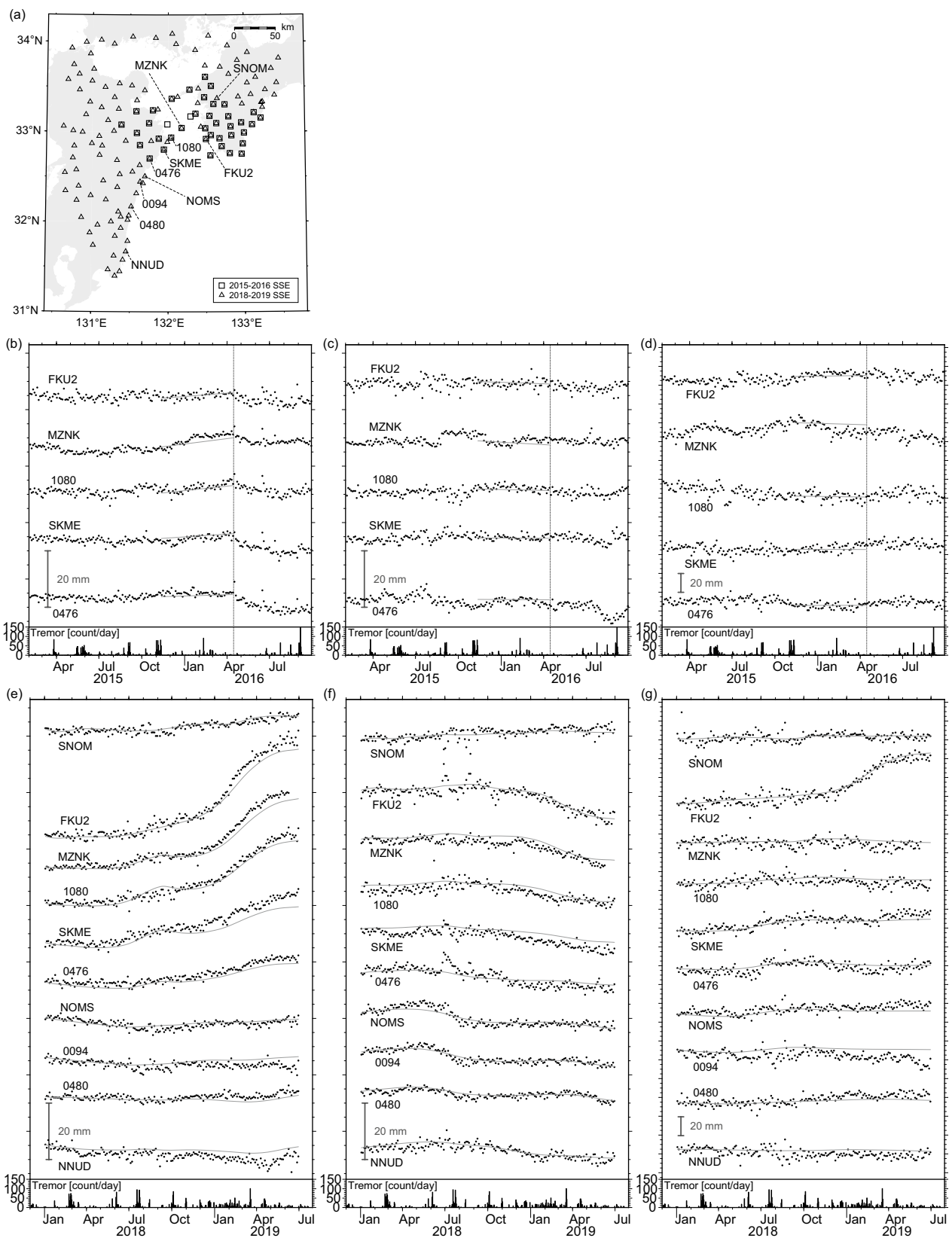
Fig. 2 (See legend on previous page.)

Hirose *et al. Earth, Planets and Space*   (2023) 75:77

Page 6 of 16

(JST) to compare the tremor catalog (Maeda and Obara 2009; Obara et al. 2010) provided by the National Research Institute for Earth Science and Disaster Resilience (NIED).

To reduce the daily scatters in the GNSS displacement time series, we calculated an averaged daily time series for the five stations in the northern part of the study area (green rectangles in Fig. 1) in IGS14 and subtracted it from the coordinate time series of all stations (e.g. Takagi et al. 2019). After the coordinates were transformed into the east, north, and upward components at each station, we estimated a linear trend, an annual variation and a semi-annual variation for each component for each station for the two time intervals: (1) from 1 January 2017 to 1 January 2018; and (2) from 1 October 2019 to 1 October 2020; to avoid the inclusion of the deformation due to the SSEs in 2018–2019 (we assumed the same velocity and coefficients of the trigonometric terms for the two time intervals). We then subtracted it from each component time series. Instantaneous offsets caused by station maintenance (e.g. antenna replacements) and large earthquakes (16 April 2016 Kumamoto, M_j 7.3, and 10 May 2019 Hyuganada, M_j 6.3; Fig. 1) were removed by estimating the difference between the two averages for 10 days just before and after the earthquake origin date or the maintenance date (M_j: the magnitude of an earthquake determined by the Japan Meteorological Agency (JMA)). The detrended daily coordinates were finally downsampled to obtain a dataset with a three-day sampling interval by calculating the mean every three days.

Figure 2 shows the processed time series data at the selected stations. A slow and small eastward transient displacement appears to start in December 2015 and to continue until February–March 2016, particularly at stations FKU2, MZNK, and 1080 (Fig. 2b). Additionally, transient subsidence appears during this period at station MZNK (Fig. 2d). The eastward displacement and subsidence at MZNK are 6 and 12 mm, respectively, and this displacement is the largest among all the stations for this time period (Fig. 3a, b). Ozawa (2017) identified the transient deformation caused by an SSE near Cape Ashizuri from 1 February to 10 April 2016 using GEONET. We assumed that the observed deformation was ascribed to the same SSE reported in Ozawa (2017), and we selected a longer time period to be analyzed than the probable duration of the SSE, such as from 10 November 2015 to 15 April 2016. Note that this end date was just before the mainshock of the Kumamoto earthquake to avoid contamination of the postseismic deformation (Fig. 2b) of the earthquake. We also selected 40 GNSS stations to be used in the inversion analysis for the SSE by visual inspection of the displacement time series plots, as shown in Fig. 2 in order to include as many stations as

possible, such that the displacement probably caused by the SSE was observed (Fig. 2a).

Around April–May 2018, another slow but much larger transient deformation appears to start and to last until June 2019 (Fig. 2e–g). This deformation episode appears to comprise two stages: (1) a smaller eastward displacement around April–May 2018, especially at stations in the Bungo Channel and the Oita area in Kyushu (e.g. MZNK, 1080, and SKME in Fig. 2e), and a southward displacement in the Miyazaki area in Kyushu (e.g. NOMS, 0094, and 0480 in Fig. 2f); (2) acceleration around December 2018 in and around the Bungo Channel (e.g. horizontal components at FKU2, MZNK, 1080, and SKME in Fig. 2e, f, and an uplift around Cape Ashizuri; e.g. FKU2 in Fig. 2g). To estimate the probable changes in the slip region throughout the entire sequence of this episode as suggested from the aforementioned observed data, we used the data of stations in a much wider area than those for the SSE in 2015–2016 for the period from 1 January 2018 to 2 July 2019. The number of selected stations is 140 (Fig. 2a).

Methods

We applied a network inversion filter (NIF; Segall and Matthews 1997) to the preprocessed time series data. This technique is based on a Kalman filter and enables the estimation of the time-dependent slip and slip rate on faults from the time series data of a network of surface deformation measurements. We used an implementation that was originally developed for tiltmeter records (Hirose and Obara 2010) based on the state-space expression proposed by Ozawa et al. (2001) and was extended for GNSS data by Hirose et al. (2014). The details of the method is described in Additional file 1: Text S1, and here we present a summary and conditions of the data analysis.

Each displacement component at each station at each time epoch is modeled as the sum of the elastic deformation due to slip on subfaults, random white noise, and random-walk noise (with a scale parameter τ). Three displacement components were analyzed with relative weights of (east, north, up) = (3:3:1), which are realized by assuming 9 times larger variance for vertical components than those for horizontal components (diagonal elements of the observation data covariance matrix Σ in equation (S10) in Additional file 1: Text S1). The difference in slip rate on a subfault at successive time epochs t_n and t_{n-1} was assumed to follow a Gaussian distribution with zero mean and variance α^2.

We assume that slow slip occurs on the plate interface on the subducting Philippine Sea plate. A spatial slip distribution is represented by a set of slip on 11×19 square subfaults with a uniform area of 15×15 km^2, which
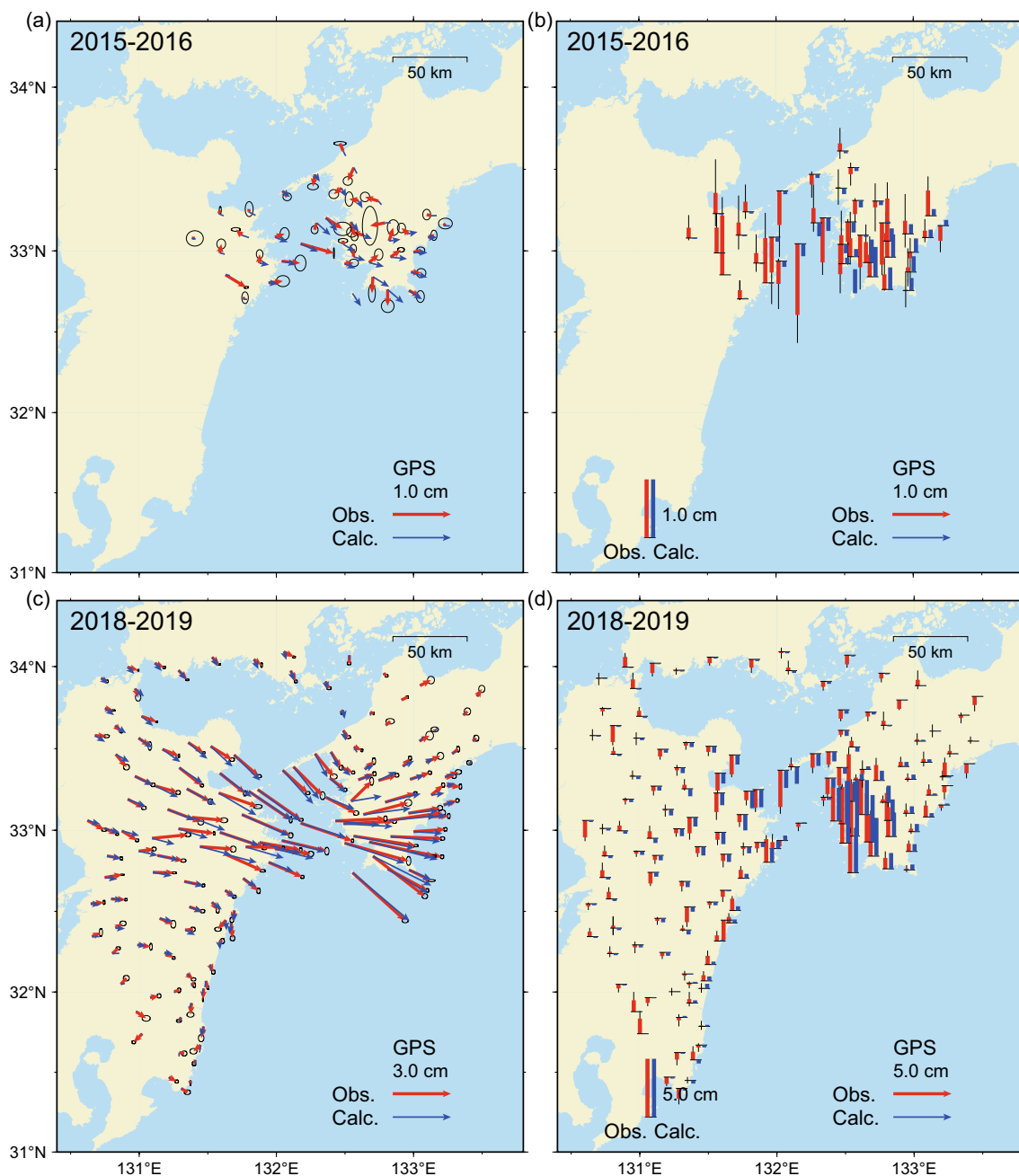
Fig. 3 Observed (red) and synthetic (blue) displacement vectors with error ellipses (one standard deviation) for the two SSEs. **a**, **b** The SSE in 2015–2016 and **c**, **d** the 2018–2019 sequence. **a**, **c** Horizontal components and **b**, **d** vertical components. The difference between the averages of coordinates for each of the first and last 15 days of the analyzed time period is calculated for each component at each station

are placed on the plate interface geometry proposed by Nakanishi et al. (2018) and Nakajima and Hasegawa (2007) (Fig. 4). For the SSE in 2015–2016, the northern subset of these subfaults (11 × 10) is used (gray rectangles in Fig. 4). On each subfault, the slip and the slip rate are uniform at each time epoch, and the slip direction (rake) is fixed such that the surface projection of the slip vector

is in the opposite direction to the relative plate motion of the Philippine Sea plate with respect to the Amurian plate (Miyazaki and Heki 2001). Synthetic surface displacements at each GNSS station are calculated using Okada (1992)'s analytical expressions assuming a homogeneous elastic half-space. We apply a non-negative constraint to the slip rate. The spatial smoothness constraint is applied

Hirose *et al. Earth, Planets and Space*   (2023) 75:77

Page 8 of 16
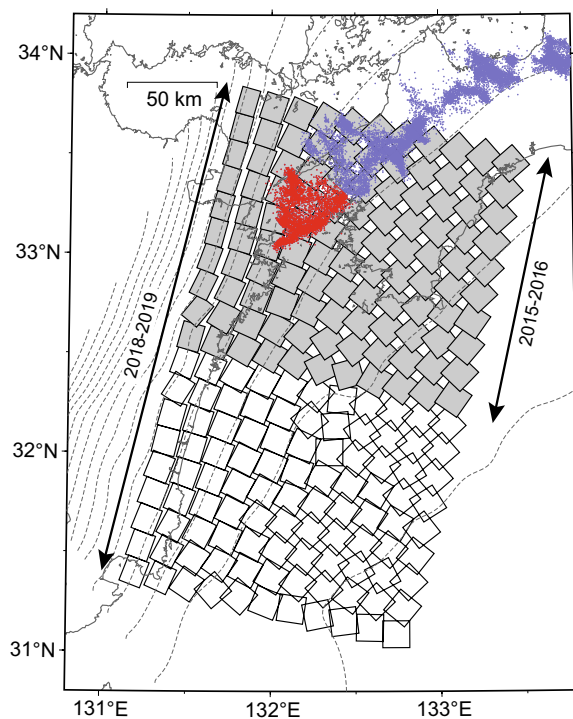
Fig. 4 Configuration of the modeled fault area. Gray rectangles represent the subfaults for the SSE in 2015–2016, whereas open and gray rectangles represent those for the 2018–2019 sequence, respectively. Red and blue dots represent the deep tremor epicenters. Tremor activity in the red area is shown in Fig. 6

to the slip rate distribution (with a scale parameter γ). Additionally, the slip rate on the outermost subfaults is constrained close to zero. Hyperparameters (α^2, τ^2, γ^2) are optimized using a maximum likelihood method.

Before applying this method to actual observation data, we first conducted a checkerboard resolution test. A slip distribution with a checkerboard pattern was used (Additional file 1: Fig. S1a) and a time function of cumulative slip was expressed as a ramp function with a duration of 7 months and a final slip amount of 20 cm. We calculated the synthetic displacement time series at all stations (Fig. 2a) and then added white noise (standard deviations of 1 and 3 mm for the horizontal and vertical components, respectively) and random-walk noise (a scale parameter of 1 mm yr$^{-1/2}$ for all components). These data were treated as observational data, and the NIF was applied to the data to retrieve an estimated source time process on the defined subfaults. Additional file 1: Figure S1b shows the estimated slip distribution from the resolution test. The distribution of the given slip patches is well recovered in the northern half of the modeled area and near the eastern coastline of Kyushu in the southern half. The eastern and central parts of the southern half are not well resolved.

Results

We applied the NIF to two time periods: (1) from 10 November 2015 to 15 April 2016 (SSE in 2015–2016); (2) from 1 January 2018 to 2 July 2019 (the 2018–2019 sequence). Figure 5a shows the final slip distribution of the SSE in 2015–2016 and Additionl file 1: Fig. S2a shows the corresponding error distribution. For this episode, we did not obtain a significant time-dependent slip process because of its small surface displacements (Fig. 6a displays the estimated cumulative moment, showing an approximately linear time function for comparison). Therefore, we will not discuss the time-dependent slip behavior of this episode but the final slip distribution. A slip patch is centered just west of Cape Ashizuri and is approximately 50 km in diameter. The northern end of the slip area does not overlap with the ETS zone. The released seismic moment is 2.6×10^{18} Nm (the corresponding moment magnitude M_w 6.2) and the maximum slip is 3.7 cm. Note that a synthetic test (Additional file 1: Text S2) supports that the estimated slip distribution is plausible.

The obtained slip distribution explains most of the characteristics in the observed spatial displacement distribution, especially the horizontal displacements (Fig. 3a). However, the synthetic displacements do not fit the smaller and shorter fluctuations in the time series (Fig. 2b–d). Large misfits appear in the vertical displacements at western stations in the station distribution (Fig. 3b), especially for the observed uplifts in the Kyushu area. If we explain these uplifts as the result of plate interface slip, deeper slip (deeper than approximately 80 km depth) on the northwest part outside the modeled fault area is required. This depth corresponds to temperature of over 800°C (Ji and Yoshioka 2017) meaning that most geologic materials exhibit velocity strengthening friction or plastic flow (e.g. Scholz 2019), and a spontaneous slip event is unlikely to occur. As this possibility is unlikely, we judged the apparent uplifts as the residuals from insufficient preprocessing, noise, or deformation from other sources.

For the 2018–2019 sequence, the final slip distribution and the corresponding error distribution are shown in Fig. 5b and Additionl file 1: Fig. S2b, respectively. At least three slip patches are apparent (also shown in Additionl file 1: Fig. S3): the first is in and around the Bungo Channel (Patch A), the second is around the Miyazaki area (Patch B), and the third is off the south of Cape Ashizuri (Patch C). Slip patch A is centered at the central part of the Bungo Channel and stretches between both sides of the Bungo Channel, i.e., the Kyushu side to the west and the Shikoku side to the east. The depth of the slip area ranges from approximately 25 to 60 km. The northern end of the slip area overlaps with the ETS zone. The
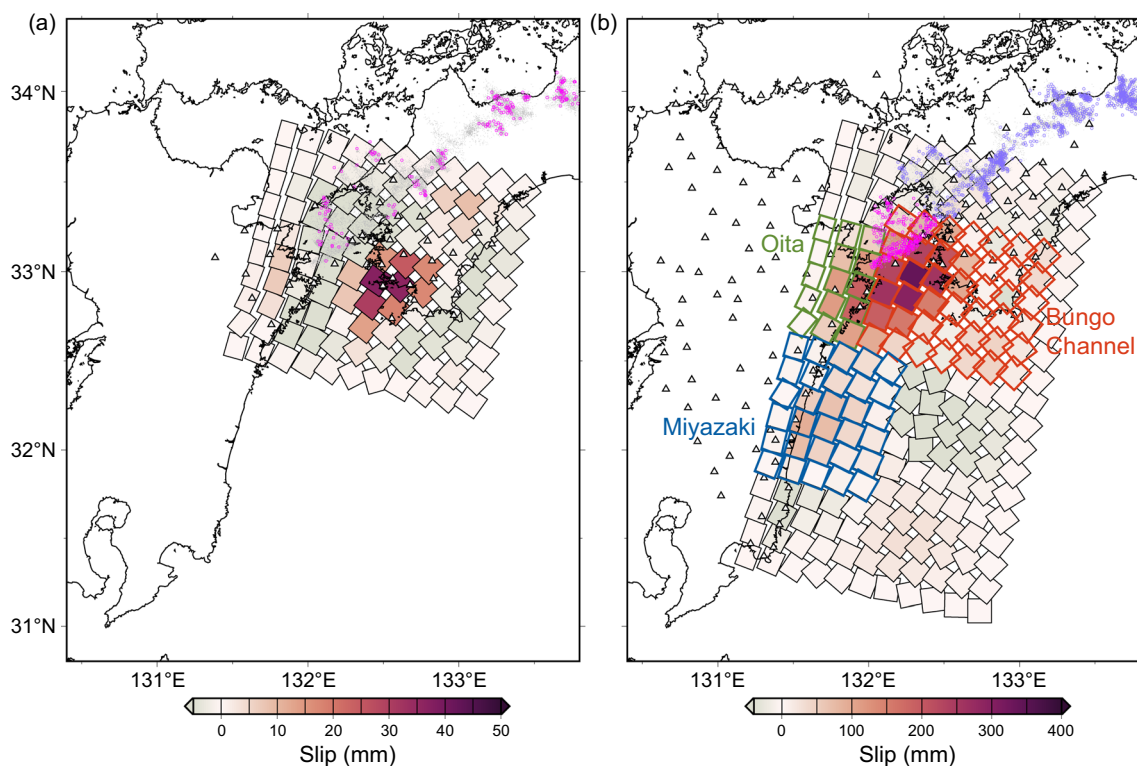
Fig. 5 Final slip distributions for the two sequences. **a** The SSE in 2015–2016 and **b** the 2018–2019 sequence. Gray dots represent tremor epicenters for the entire period (2001–2020), whereas magenta circles in (**a**) and magenta and blue circles in (**b**) show the tremors during each SSE time period. The cumulative number of tremors denoted as magenta circles is displayed in Fig. 6b. Red, green, and blue subfaults in (**b**) denote the sub-areas for calculating the cumulative moment time series shown in Fig. 6b

released seismic moment of the slip patch is 3.7×10^{19} Nm (M_w 7.0) and the maximum slip is 34 cm. Since this patch corresponds to the area of the recurrent Bungo Channel SSEs (e.g. Hirose et al. (1999); Ozawa et al. (2001, 2020); Seshimo and Yoshioka (2022)), we identified as the fourth major Bungo Channel long-term SSE following SSEs in 1997, 2003, and 2010. Slip patch B is located in the Miyazaki area and is adjacent to patch A on the southern side. Its diameter is approximately 50 km and its depth ranges from approximately 25 to 40 km. The seismic moment released from this slip patch through this episode is 6.5×10^{18} Nm (M_w 6.5) and the maximum slip is 9.2 cm. This patch corresponds to the slip area of recurrent SSEs around the Miyazaki area (Yarai and Ozawa 2013; Ozawa 2017; Takagi et al. 2019). Slip patch C is located east of slip patch A, south and east of Cape Ashizuri, and appears to distribute along the 20 km isodepth contour of the subducting Philippine Sea plate. Its depth is significantly shallower than those of the other two slip patches. This slip area is adjacent to and may partly overlap the source area of the 1946 Nankai earthquake (Fig. 1). The seismic moment of this patch is 3.0×10^{18} Nm (M_w 6.3) and the maximum slip is 4.7 cm. This

patch could correspond to a shallow invading slip in the locked megathrust zone proposed by Kano et al. (2019).

The slip process of the 2018–2019 sequence shows a clear time evolution (Fig. 7, Additional file 2: Movie S1; the corresponding error distributions are shown in Additionl file 1: Fig. S4). The slip seems to start beneath the Oita area around April 2018 and gradually increases. In May 2018, the slip begins to propagate southward. The slip beneath the Oita area appears to cease in October 2018, but that around Miyazaki area continues until around March 2019. Conversely, the slip also starts to propagate to the east toward the central part of the Bungo Channel from the Oita area in June 2018. This slip propagates through the southern shallower part of the Bungo Channel and appears to reach slip patch C around August 2018. Around November 2018, the slip accelerates in patch A, which is the main slip area of the Bungo Channel SSEs. The slip rate reaches its maximum in February 2019, and the slip continues until June 2019 with a decreasing slip rate.

We also identified three short-term SSEs in the western Shikoku area in February 2018, October 2018, and March 2019 (Fig. 7; event IDs "201802", "201810",
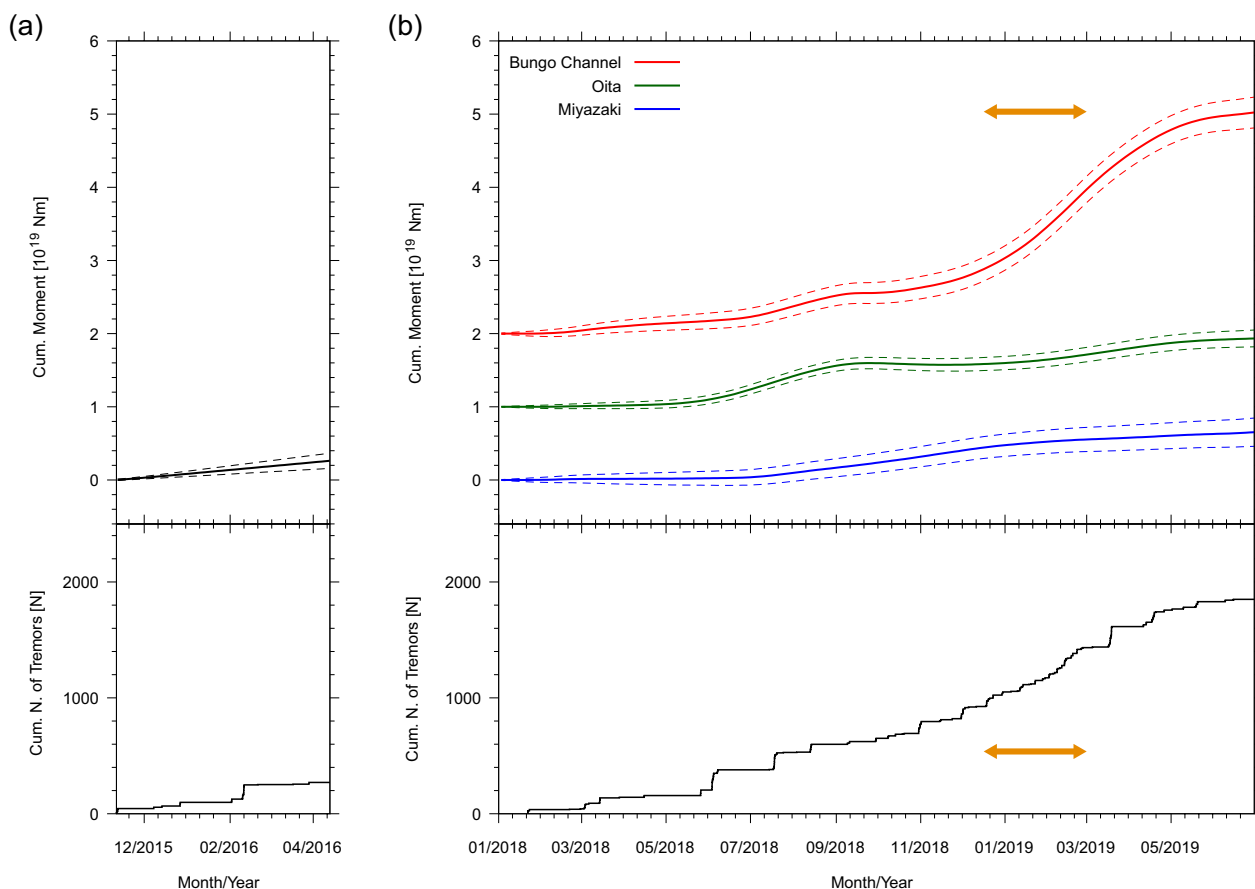
Fig. 6 Cumulative moment (top) and cumulative number of deep tremors (bottom) for **a** the SSE in 2015–2016 and **b** the 2018–2019 sequence. Cumulative moment in (**a**) shows that on the whole subfault area (gray rectangles in Fig. 4), whereas the cumulative moment in (**b**) shows those in three areas ("Bungo Channel", "Oita", and "Miyazaki") depicted in Fig. 5b. Tremors in (b, bottom) correspond to those denoted as magenta circles in Fig. 5b. Orange arrows in (b) shows the acceleration phase of the SSE. Note that each trace in (b, top) is arbitrarily shifted in the vertical direction for clarity

"201903" in Hirose and Kimura 2020). The estimated temporal variation of the slip is too smooth for discussing the slip process of a short-term SSE with a week-long duration because the main objective of this study is to estimate long-term (year-long) interplate slip behaviors and therefore the temporal and spatial smoothnesses are optimized to these behaviors. But we can obtain approximate timing, spatial location, and magnitude of these slip episodes. Event 201802 started 21 February 2018 and continued for 32 days (Hirose and Kimura 2020). As we described above, the long-term slip seems to start around April 2018 in the Oita area, adjacent to the source area of the episode 201802. Event 201810 occurred on 30 September 2018 and lasted for 8 days (Hirose and Kimura 2020). This episode occurred immediately after the slip propagated from west to east between June and August 2018 and was close to the acceleration phase of the long-term SSE. Event 201903 occurred on 2 March 2019 and lasted for six days (Hirose and Kimura 2020). This time

interval was during the main phase of the long-term SSE adjacent to the slip area of the event 201903.

Figures 6b and Additionl file 1: Fig. S5 show the cumulative seismic moment and the moment rate functions on the three areas displayed in Fig. 5b during the 2018–2019 sequence. The moment release histories for each area corresponds to the aforementioned spatiotemporal slip process. A small increase in the moment release in the Bungo Channel around March 2018 (red curve in Fig. 6b and Additionl file 1: Fig. S5) corresponds to the ETS SSE 201802. Subsequently, a longer transient moment release starts in the Oita area (green curve in Fig. 6b and Additionl file 1: Fig. S5) around April 2018, followed by an increase in the moment around June 2018 in the Bungo Channel. Simultaneously, a moment release begins in the Miyazaki area (blue curve in Fig. 6b and Additionl file 1: Fig. S5), corresponding to the southward slip propagation and a long-term SSE in Miyazaki. An acceleration in the moment release appears around November 2018, mainly
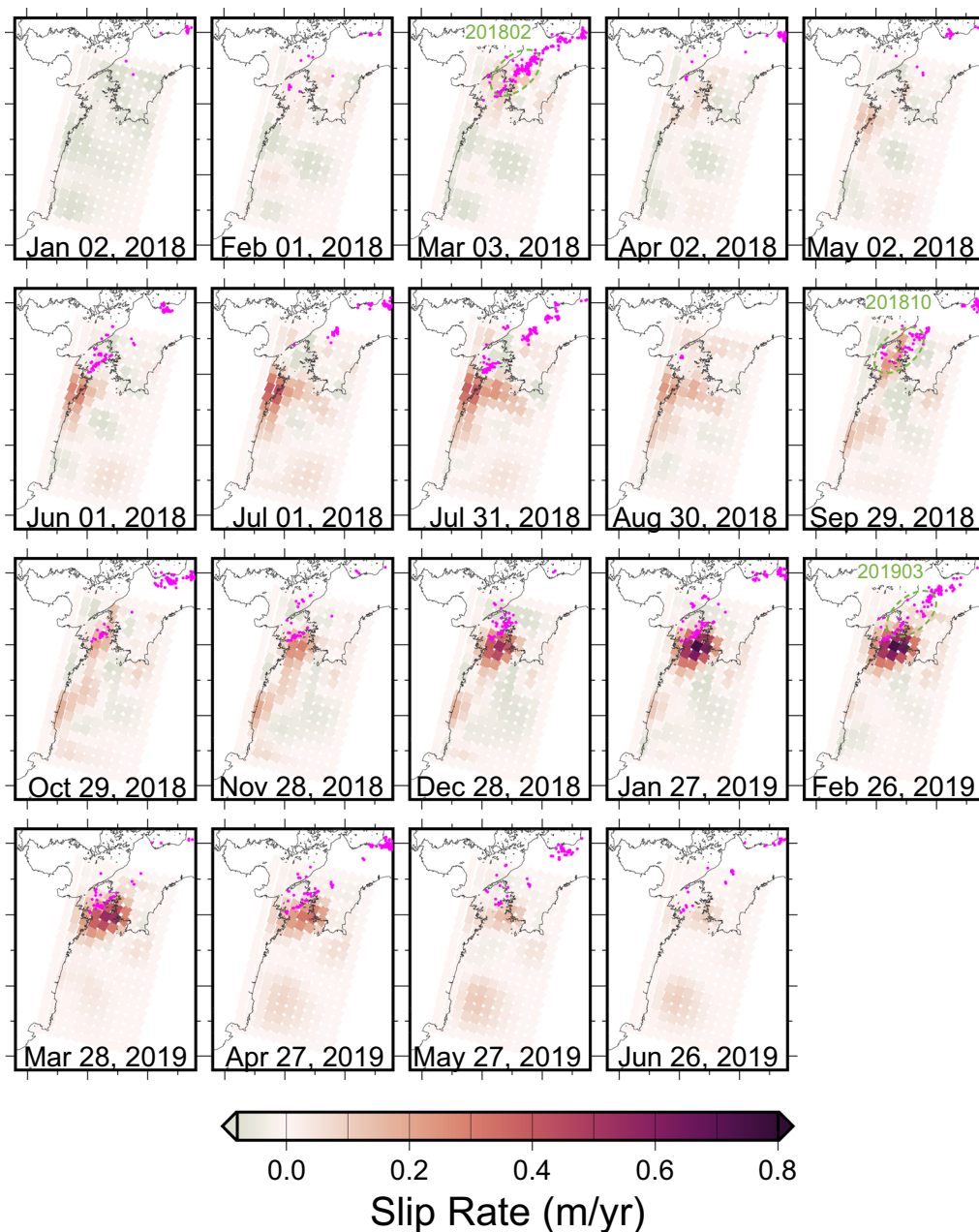
Fig. 7 Snapshots of slip rate distributions for every 30 days for the 2018–2019 sequence. Magenta dots show epicenters of deep tremors that occurred during each 30-day time window centered at the displayed date. Green dashed ellipses show the slip areas of detected short-term SSEs with event IDs defined in Hirose and Kimura (2020)

in the Bungo Channel, and the moment release continues until June 2019. The cumulative number of deep tremors in the Bungo Channel (bottom panel in Fig. 6b) shows a clear gradual increase from around December 2018 to March 2019 (arrow in Fig. 6b, bottom), which corresponds to the acceleration phase of the slow slip in the Bungo Channel, in addition to several short-term activations probably corresponding to ETS episodes.

Figures 3c,d show a comparison of the observed displacement vectors with the synthetic vectors through the 2018–2019 sequence. The fitting of the synthetic data to the observed data is reasonably good. The synthetic displacement time series explain most of the long-term features appearing in the observed surface displacements (Fig. 2e–g).

Discussion

The slip areas of the two SSE episodes show distinct differences in terms of the spatial and temporal relationships with the deep tremor zone. The slip area of the SSE in 2015–2016 is limited to the southeast part of the main slip area of the 2018–2019 Bungo Channel SSE (patch A in Additionl file 1: Fig. S3) and does not overlap the ETS zone (Figs. 5a, 8). There is no indication of activated tremors spanning several months in correlation with the SSE in 2015–2016, although a tremor activity lasting for approximately two days occurred in February 2016 (Fig. 6a, bottom). Conversely, slip occurs in most parts of patch A, especially after the acceleration phase of the 2018–2019 SSE and overlaps the ETS zone (Figs. 5b, 8). This acceleration phase is temporally well correlated with the gradual increase in the number of tremors occurring in the Bungo Channel (Fig. 6b). Similar synchronization of the deep tremor activity and the acceleration phase of the long-term SSE are observed in 2003 and 2010 (Hirose et al. 2010). This suggests that the tremor activity is directly triggered by a long-term SSE that propagates into the ETS zone.
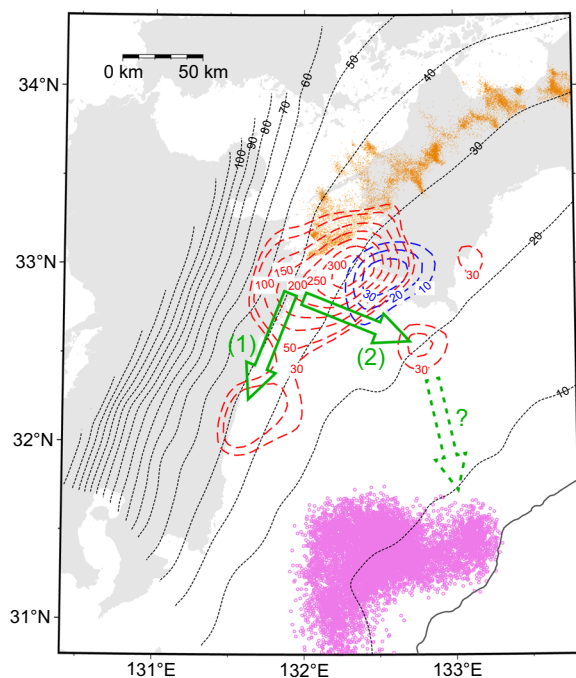
Fig. 8 Comparison of the slip distributions for the two studied SSEs. Blue and red dashed curves show contours of the final slip distributions for the SSE in 2015–2016 and the 2018–2019 sequence, respectively. Numbers are in mm. Orange dots, pink circles and broken lines are the same as in Fig. 1. Green arrows with numbers indicate major slip propagation paths during the 2018–2019 sequence. The dashed green arrow shows a possible slip propagation path

The estimated slip distributions also show differences in the depth (Fig. 8). The slip area for the SSE in 2015–2016 ranges between depths of 20 and 30 km, whereas three slip patches are identified for the 2018–2019 sequence with different depth ranges, as described above. From the time evolution of the 2018–2019 sequence, the slip process in patch A is divided into two stages, as shown in Ozawa et al. (2020) and Seshimo and Yoshioka (2022): the first stage in the western part (Oita area) spanned from around April 2018 to around October 2018 and the second stage for the rest of the patch (main part) in the Bungo Channel extended from around November 2018 to June 2019 (Figs. 6b, 7). Most of the slip area of the first stage corresponds to an area deeper than 40 km, and that of the second stage ranges from a depth of 25 to 40 km (Fig. 8). The latter depth range is almost the same as that of patch B around the Miyazaki area. In addition, Seshimo and Yoshioka (2022) pointed out that the 2002–2004 SSE in the Bungo Channel had a source process similar to that of the 2018–2019 SSE. These lines of evidence suggest that patch A comprised two parts: the deeper Oita area and the main Bungo Channel area. The main part shares similar physical properties with long-term SSEs in the surrounding area (e.g. Takagi et al. (2019)), but the deeper part may have a different frictional property; thus, the slip process is not a simple one such as its moment rate function having only one peak, but has two separate stages.

The 2018–2019 sequence also has a third shallower patch C (Figs. 8, 5, Additionl file 1: Fig. S3). This patch likely corresponds to an additional shallower slip area during deep ETS episodes found from a GNSS time series stacking of multiple ETS episodes (Kano et al. 2019). Kano et al. (2019) interpreted that the shallower slip invaded into the shallower locked megathrust zone from the ETS zone. Conversely, we found that the slip propagates from the deeper Oita area to the shallower patch C through the southern part of the Bungo Channel, and the shallower slip lasts for over eight months (Fig. 7, Additional files 1, 2: Fig. S6, Movie S1). During the propagation and duration, two short-term ETS episodes occurred in the western Shikoku area. This indicates the possibility that the shallower slip did not propagate directly from the deeper ETS zone within short-term ETS episodes but was a long-lasting slip that propagated from the west, namely, from the Bungo Channel.

In addition, Hirose et al. (2010) showed the simultaneous occurrence of a Bungo Channel SSE, deep tremor, and shallow VLFEs, and suggested the presence of a possible shallower slip extending from the Bungo Channel SSE area to the shallow VLFE area far south of Cape Ashizuri. Although this study does not have enough resolution to study the area further south of the shallower

slip patch C, it might possibly explain the simultaneous occurrence as the slip at patch C could propagate to the area further south toward the shallow VLFE area (Fig. 8). However, National Research Institute for Earth Science and Disaster Resilience (2020) reported no activation of shallow VLFEs during the 2018–2019 sequence in the area far south of Cape Ashizuri, where VLFE activations were observed in correlation with the Bungo Channel SSEs, although some activities occurred in Hyuganada in August and October 2018 (National Research Institute for Earth Science and Disaster Resilience 2019). The absence of VLFE activity suggests that the slip did not propagate further south from patch C during the 2018–2019 sequence.

Another interesting feature of the 2018–2019 sequence is a clear slip propagation from the Oita area to the south, namely, the Miyazaki area, at a speed of the order of 1 km/day (Additionl file 1: Fig. S7). This directly connects the source areas of the two long-term SSEs: the Bungo Channel SSEs (e.g. Hirose et al. (1999)) and the Miyazaki SSEs (e.g. Yarai and Ozawa (2013)). The observed displacements indicate this southward propagation. For example, station 0476 appears to start a southward displacement around April 2018, NOMS and 0094 around May, and 0480 around June, indicating that the onset time of the deformation is gradually delayed from the northern to the southern stations (Fig. 2f). Takagi et al. (2019) show along-strike migrations of source areas of SSEs from south to north at an average speed of 50–200 km/year. Uchida et al. (2020) also show a similar northward migration at a similar speed in the Hyuganada area from the analysis of repeating earthquakes located updip of the SSE zone (corresponding to a depth of 15–30 km), shallow VLFEs, and deep ETS tremor. They also indicate a "fast migration" during the 2010 Bongo Channel SSE in the same area. In this migration, seismic and aseismic (SSE) activities in a large area with a length of approximately 300 km sequentially occur from south to north within approximately one month. This speed (∼1 km/day) approximately corresponds to that of the southward propagation of the slow slip found in our study. The similar propagation speeds suggest that the slip propagations of the deeper slow slip and the possible shallower slip that drives repeating earthquakes and VLFEs are controlled by a common or similar physical mechanism and/or are generated under similar physical conditions. However, the southward slip propagation is the opposite direction that is proposed by Uchida et al. (2020). This is another propagation mode in the deeper zone on the plate interface in Hyuganada. It is well known that deep ETS episodes propagate in both directions along the strike of a subduction zone [e.g. Obara (2002); Hirose and Obara (2010)], although there are some characteristic

tendencies [e.g. Obara et al. (2010)]. Hence, it is important to observe more migration/propagation episodes to determine the tendency of slip propagation directions and subsequently explore the factors determining such a tendency.

The spatial and temporal relationship between long-term and short-term SSEs is important for understanding the possible interaction between them. Hirose and Obara (2005) showed that the recurrence interval of short-term SSEs in the western Shikoku area shortened during and after the long-term SSE in the Bungo Channel in 2003–2004. As described above, temporal and spatial variations in the slip are too smooth to discuss the slip process of a short-term SSE; however, the timing of the occurrence of short-term SSEs might indicate possible causal connections between short-term SSEs and slip stages in the 2018–2019 episode (Fig. 7). First, just after the short-term SSE 201802, the slip seems to have started in the Oita area. Second, event 201810 occurred just after the eastward slip propagation to patch C. Third, slip started to accelerate in patch A after event 201810. Fourth, event 201903 occurred during the main slip stage in patch A. Further studies with finer temporal and spatial resolutions are required to investigate this relationship.

Conclusions

Based on long-term observations at our original continuous GNSS stations in addition to the GSI GEONET stations, we observed crustal deformations of two sequences of slow slip episodes around the Bungo Channel and Hyuganada. One was a smaller SSE in 2015–2016 and the other was a 2018–2019 sequence that included a larger long-term SSE in the Bungo Channel and an SSE around the Miyazaki Plain.

Time-dependent slip inversion analyses of the observed crustal deformation data for both sequences show that the slip area for the SSE in 2015–2016 is a smaller area centered just west of Cape Ashizuri and does not extend to the ETS zone to the north. However, that in 2018–2019 starts near the Oita area and propagates to the Bungo Channel to the east and reaches to the ETS zone. Tremor is activated when the slow slip propagates to the ETS zone for the 2018–2019 sequence, whereas no clear coincidence of slow slip and tremor activity is observed for the SSE in 2015–2016. This strongly suggests that synchronized tremor activity with an SSE requires slip close to or overlapping the ETS zone.

During the 2018–2019 sequence, two significant slip propagations are observed: (1) a southward propagation along a deeper part from the Oita area to the Miyazaki area and (2) an eastward propagation from the Oita area to the shallower Cape Ashizuri area. The first propagation shows a clear connection between the Bungo Channel

Hirose *et al. Earth, Planets and Space* (2023) 75:77

Page 14 of 16

SSE area and the Miyazaki Plain SSE area, and a propagation direction opposite to that proposed by Uchida et al. (2020) in Hyuganada and around the Bungo Channel. The second propagation provides another scenario for the slow slip invading the megathrust zone (Kano et al. 2019). This study demonstrates new propagation modes in the deeper zone of Hyuganada and from the deeper to shallower parts around the Bungo Channel area.

Abbreviations

JPL	Jet Propulsion Laboratory
GNSS	Global navigation satellite system
GEONET	GNSS Earth Observation System
GPS	Global positioning system
SSE	Slow slip event
ETS	Episodic tremor and slip
NIED	National Research Institute for Earth Science and Disaster Resilience
GSI	Geospatial Information Authority of Japan
IGS	International GNSS Service
GMT	The Generic Mapping Tools
RINEX	Receiver Independent Exchange Format
JST	Japan Standard Time
JMA	Japan Meteorological Agency
NIF	Network inversion filter
VLFE	Very low-frequency earthquake

Supplementary Information

The online version contains supplementary material available at https://doi.org/10.1186/s40623-023-01833-4.

Additional file 1 : Text S1. A Network Inversion Filter implementation used in this study. **Text S2**. A synthetic test for the 2015–2016 SSE. **Figure S1**. A checkerboard resolution test. **a** Given slip distribution. **b** Estimated slip distribution. **Figure S2**. Error distributions of slip for **a** the 2015–2016 SSE; and **b** the 2018–2019 sequence. Standard deviations for each subfault is displayed. **Figure S3**. The final slip distribution for the 2018–2019 sequence that is the same as in Figure 5. This map indicates indices for slip patches. **Figure S4**. Error distributions of slip rates for the 2018–2019 sequence. Standard deviations for each subfault is displayed. **Figure S5**. Moment rate functionsand cumulative number of deep tremorsfor the 2018–2019 sequence corresponding to Figure 6. Moment rate functions for the three areas depicted in Figure 5 are shown. Traces in the top frame are arbitrarily shifted vertically for clarity. The bottom trace is the same one as in the bottom frame of Figure 6b. **Figure S6**. Slip rate time functions at subfaults on the 12th rawfor the 2018–2019 sequence. Horizontal axis denotes time in date/month. Traces from bottom to top are at subfaults from west to east. Approximate distance from the westernmost subfault is shown on the left vertical axis. Inverted triangles show approximate arrival times of the slip propagation front from Oita to the east in 2018 at each subfault. Thick dashed line shows a fitted line to the arrival times showing a slip propagation speed of ∼0.6 km/day. **Figure S7**. Slip rate time functions at subfaults on the third columnfor the 2018–2019 sequence. Horizontal axis denotes time in date/month. Traces from bottom to top are at subfaults from south to north. Approximate distance from the southernmost subfault is shown on the left vertical axis. Inverted triangles show approximate arrival times of the slip propagation front from Oita to the south in 2018 at each subfault. Thick dashed line shows a fitted line to the arrival times showing a slip propagation speed of 1 km/day. **Figure S8**. A synthetic test simulating the simplified slip distribution of the 2015–2016 SSE. **a** Given slip distribution. **b** Estimated slip distribution.

Additional file 2 : Movie S1. Slip rate distributions for every 3 days for the 2018-2019 sequence.

Author details

[1]Research Center for Urban Safety and Security, Kobe University, 1-1 Rokkodai-cho, Nada, Kobe 657-8501, Japan. [2]Institute of Seismology and Volcanology, Faculty of Science, Kyushu University, 2-5643-29 Shinyama, Shimabara, Nagasaki 855-0843, Japan. [3]Faculty of Science and Technology, Kochi University, 2-5-1 Akebonocho, Kochi, Kochi 780-8520, Japan. [4]Disaster Prevention Research Institute, Kyoto University, Gokasho, Uji, Kyoto 611-0011, Japan.

References

Ando M (1975) Source mechanisms and tectonic significance of historical earthquakes along the Nankai Trough, Japan. Tectonophysics 27(2):119–140. https://doi.org/10.1016/0040-1951(75)90102-X

Asano Y, Obara K, Ito Y (2008) Spatiotemporal distribution of very-low frequency earthquakes in Tokachi-oki near the junction of the Kuril and Japan trenches revealed by using array signal processing. Earth Planet Space 60(8):871–875. https://doi.org/10.1186/BF03352839

Asano Y, Obara K, Matsuzawa T, Hirose H, Ito Y (2015) Possible shallow slow slip events in Hyuga-nada, Nankai subduction zone, inferred from migration of very low frequency earthquakes. Geophys Res Lett 42(2):331–338. https://doi.org/10.1002/2014GL062165

Hirose H, Kimura T (2020) Slip distributions of short-term slow slip events in Shikoku, Southwest Japan, From 2001 to 2019 based on tilt change measurements. J Geophys Res Solid Earth 125(6):e2020JB019601. https://doi.org/10.1029/2020JB019601

Hirose H, Obara K (2005) Repeating short- and long-term slow slip events with deep tremor activity around the Bungo channel region, southwest Japan. Earth Planet Space 57(10):961–972. https://doi.org/10.1186/BF03351875

Hirose H, Obara K (2010) Recurrence behavior of short-term slow slip and correlated nonvolcanic tremor episodes in western Shikoku, southwest

Japan. J Geophys Res 115(B00A21):10. https://doi.org/10.1029/2008JB006050

Hirose H, Hirahara K, Kimata F, Fujii N, Miyazaki S (1999) A slow thrust slip event following the two 1996 Hyuganada Earthquakes beneath the Bungo Channel, southwest Japan. Geophys Res Lett 26(21):3237–3240. https://doi.org/10.1029/1999GL010999

Hirose H, Asano Y, Obara K, Kimura T, Matsuzawa T, Tanaka S, Maeda T (2010) Slow earthquakes linked along dip in the Nankai subduction zone. Science 330(6010):1502. https://doi.org/10.1126/science.1197102

Hirose H, Matsuzawa T, Kimura T, Kimura H (2014) The Boso slow slip events in 2007 and 2011 as a driving process for the accompanying earthquake swarm. Geophys Res Lett 41(8):2778–2785. https://doi.org/10.1002/2014GL059791

Ide S (2012) Variety and spatial heterogeneity of tectonic tremor worldwide. J Geophys Res 117(B3):B03302. https://doi.org/10.1029/2011JB008840

Ji Y, Yoshioka S (2017) Slab dehydration and earthquake distribution beneath southwestern and central Japan based on three-dimensional thermal modeling. Geophys Res Lett 44(6):2679–2686. https://doi.org/10.1002/2016GL072295

Kano M, Kato A, Obara K (2019) Episodic tremor and slip silently invades strongly locked megathrust in the Nankai Trough. Sci Rep 9(1):1–8. https://doi.org/10.1038/s41598-019-45781-0

Kimura H, Tadokoro K, Ito T (2019) Interplate coupling distribution along the Nankai Trough in southwest japan estimated from the block motion model based on onshore GNSS and seafloor GNSS/A observations. J Geophys Res Solid Earth 124(6):6140–6164. https://doi.org/10.1029/2018JB016159

Kobayashi A (2010) A small scale long-term slow slip occurred in the western Shikoku in 2005. J Seism Soc Jpn 63(2):97–100. https://doi.org/10.4294/zisin.63.97 (in Japanese)

Kobayashi A (2012) Long-term slow slip event around Kochi City from 1977 to 1980. J Seism Soc Jpn 64(2):63–73. https://doi.org/10.4294/zisin.64.63 (in Japanese with English Abstract)

Maeda T, Obara K (2009) Spatiotemporal distribution of seismic energy radiation from low-frequency tremor in western Shikoku, Japan. J Geophys Res 114:17. https://doi.org/10.1029/2008JB006043

Miyazaki S, Heki K (2001) Crustal velocity field of southwest Japan: Subduction and arc-arc collision. J Geophys Res Solid Earth 106(B3):4305–4326. https://doi.org/10.1029/2000JB900312

Nakajima J, Hasegawa A (2007) Subduction of the Philippine Sea plate beneath southwestern Japan: slab geometry and its relationship to arc magmatism. J Geophys Res 112:18. https://doi.org/10.1029/2006JB004770

Nakanishi A, Takahashi N, Yamamoto Y, Takahashi T, Ozgur Citak S, Nakamura T, Obana K, Kodaira S, Kaneda Y (2018) Three-dimensional plate geometry and P-wave velocity models of the subduction zone in SW Japan: implications for seismogenesis. In: Byrne T, Underwood MB, Fisher D, McNeill L, Saffer D, Ujiie K, Yamaguchi A (eds) Geology and tectonics of subduction zones: a tribute to Gaku Kimura, special paper, vol 534. Geological Society of America, Boulder

National Research Institute for Earth Science and Disaster Resilience (2019) Activity of shallow very-low-frequency earthquakes in and around Japan (May–October, 2018). Report of the Coordinating Committee for Earthquake Prediction 101:5–7 (in Japanese)

National Research Institute for Earth Science and Disaster Resilience (2020) Activity of shallow very-low-frequency earthquakes in and around Japan (May–October, 2019). Report of the Coordinating Committee for Earthquake Prediction 103:4–7 (in Japanese)

Nishimura T (2014) Short-term slow slip events along the Ryukyu Trench, southwestern Japan, observed by continuous GNSS. Prog Earth Planet Sci. https://doi.org/10.1186/s40645-014-0022-5

Nishimura T, Yokota Y, Tadokoro K, Ochi T (2018) Strain partitioning and interplate coupling along the northern margin of the Philippine Sea plate, estimated from Global Navigation Satellite System and Global Positioning System-Acoustic data. Geosphere. https://doi.org/10.1130/GES01529.1

Obara K (2002) Nonvolcanic deep tremor associated with subduction in southwest Japan. Science 296(5573):1679–1681. https://doi.org/10.1126/science.1070378

Obara K, Ito Y (2005) Very low frequency earthquakes excited by the 2004 off the Kii peninsula earthquakes: a dynamic deformation process in the

large accretionary prism. Earth Planet Space 57(4):321–326. https://doi.org/10.1186/BF03352570

Obara K, Hirose H, Yamamizu F, Kasahara K (2004) Episodic slow slip events accompanied by non-volcanic tremors in southwest Japan subduction zone. Geophys Res Lett 31(L23602):4. https://doi.org/10.1029/2004GL020848

Obara K, Tanaka S, Maeda T, Matsuzawa T (2010) Depth-dependent activity of non-volcanic tremor in southwest Japan. Geophys Res Lett 37(L13306):5. https://doi.org/10.1029/2010GL043679

Okada Y (1992) Internal deformation due to shear and tensile faults in a half-space. Bull Seismol Soc Am 82(2):1018–1040. https://doi.org/10.1785/BSSA0820021018

Okada Y, Nishimura T, Tabei T, Matsushima T, Hirose H (2022) Development of a detection method for short-term slow slip events using GNSS data and its application to the Nankai subduction zone. Earth Planet Space 74(1):18. https://doi.org/10.1186/s40623-022-01576-8

Ozawa S (2017) Long-term slow slip events along the Nankai trough subduction zone after the 2011 Tohoku earthquake in Japan. Earth Planet Space 69(1):56. https://doi.org/10.1186/s40623-017-0640-4

Ozawa S, Murakami M, Tada T (2001) Time-dependent inversion study of the slow thrust event in the Nankai trough subduction zone, southwestern Japan. J Geophys Res Solid Earth 106(B1):787–802. https://doi.org/10.1029/2000JB900317

Ozawa S, Kawabata R, Kokado K, Yarai H (2020) Long-term slow slip events along the Nankai trough subduction zone delayed by the 2016 Kumamoto earthquake, Japan. Earth Planet Space 72(1):61. https://doi.org/10.1186/s40623-020-01189-z

Rogers G, Dragert H (2003) Episodic tremor and slip on the Cascadia subduction zone: the chatter of silent slip. Science 300(5627):1942–1943. https://doi.org/10.1126/science.1084783

Sagiya T, Thatcher W (1999) Coseismic slip resolution along a plate boundary megathrust: the Nankai Trough, southwest Japan. J Geophys Res Solid Earth 104(B1):1111–1129. https://doi.org/10.1029/98JB02644

Scholz CH (2019) The Mechanics of Earthquakes and Faulting, 3rd edn. Cambridge University Press, Cambridge

Segall P, Matthews M (1997) Time dependent inversion of geodetic data. J Geophys Res Solid Earth 102(B10):22391–22409. https://doi.org/10.1029/97JB01795

Seshimo Y, Yoshioka S (2022) Spatiotemporal slip distributions associated with the 2018–2019 Bungo Channel long-term slow slip event inverted from GNSS data. Sci Rep 12(1):343. https://doi.org/10.1038/s41598-021-03982-6

Takagi R, Obara K, Maeda T (2016) Slow slip event within a gap between tremor and locked zones in the Nankai subduction zone. Geophys Res Lett 43:2015GL066987. https://doi.org/10.1002/2015GL066987

Takagi R, Uchida N, Obara K (2019) Along-strike variation and migration of long-term slow slip events in the western Nankai subduction zone, Japan. J Geophys Res Solid Earth 124(4):3853–3880. https://doi.org/10.1029/2018JB016738

Tonegawa T, Yamashita Y, Takahashi T, Shinohara M, Ishihara Y, Kodaira S, Kaneda Y (2020) Spatial relationship between shallow very low frequency earthquakes and the subducted Kyushu-Palau Ridge in the Hyuga-nada region of the Nankai subduction zone. Geophys J Int 222(3):1542–1554. https://doi.org/10.1093/gji/ggaa264

Uchida N, Takagi R, Asano Y, Obara K (2020) Migration of shallow and deep slow earthquakes toward the locked segment of the Nankai megathrust. Earth Planet Sci Lett 531(115):986. https://doi.org/10.1016/j.epsl.2019.115986

Wessel P, Luis JF, Uieda L, Scharroo R, Wobbe F, Smith WHF, Tian D (2019) The generic mapping tools version 6. Geochem Geophys Geosyst 20(11):5556–5564. https://doi.org/10.1029/2019GC008515

Yagi Y, Kikuchi M, Yoshida S, Yamanaka Y (1998) Source process of the Hyuga-nada earthquake of April 1, 1968 (M_{jma} 7.5) and its relationship to the subsequent seismicity. J Seism Soc Jpn 51(1):139–148. https://doi.org/10.4294/zisin1948.51.1_139 (in Japanese with English Abstract)

Yamashita Y, Shimizu H, Goto K (2012) Small repeating earthquake activity, interplate quasi-static slip, and interplate coupling in the Hyuga-nada, southwestern Japan subduction zone. Geophys Res Lett. https://doi.org/10.1029/2012GL051476

Yamashita Y, Yakiwara H, Asano Y, Shimizu H, Uchida K, Hirano S, Umakoshi K, Miyamachi H, Nakamoto M, Fukui M, Kamizono M, Kanehara H, Yamada

Hirose *et al. Earth, Planets and Space*   (2023) 75:77

Page 16 of 16

T, Shinohara M, Obara K (2015) Migrating tremor off southern Kyushu as evidence for slow slip of a shallow subduction interface. Science 348(6235):676–679. https://doi.org/10.1126/science.aaa4242

Yamashita Y, Shinohara M, Yamada T (2021) Shallow tectonic tremor activities in Hyuga-nada, Nankai subduction zone, based on long-term broadband ocean bottom seismic observations. Earth Planet Space 73(1):196. https://doi.org/10.1186/s40623-021-01533-x

Yarai H, Ozawa S (2013) Quasi-periodic slow slip events in the afterslip area of the 1996 Hyuga-nada earthquakes, Japan. J Geophys Res Solid Earth 118(5):2512–2527. https://doi.org/10.1002/jgrb.50161

Yokota Y, Ishikawa T, Si Watanabe, Tashiro T, Asada A (2016) Seafloor geodetic constraints on interplate coupling of the Nankai Trough megathrust zone. Nature 534(7607):374–377. https://doi.org/10.1038/nature17632

Publisher's Note